

# Algorithm Comparison for Oxygen Saturation Estimation in Whole Blood Using Diffuse Reflectance Hyperspectral Imaging

Michelle Bryarly<sup>a</sup>, Minh Ha Tran<sup>a</sup>, Arrsh Ali<sup>a</sup>, Ling Ma<sup>a,b</sup>, Baowei Fei<sup>a,b,c\*</sup>

<sup>a</sup>Department of Bioengineering, University of Texas at Dallas, Richardson, TX, USA

<sup>b</sup>Department of Radiology, University of Texas Southwestern Medical Center, Dallas, TX, USA

<sup>c</sup>Center for Imaging and Surgical Innovation, University of Texas at Dallas, Richardson, TX, USA

\*Corresponding author: [bfei@utdallas.edu](mailto:bfei@utdallas.edu), Website: <https://fei-lab.org>

## ABSTRACT

Hyperspectral imaging (HSI) has been used *in vivo* to estimate the oxygenation level (SO<sub>2</sub>) of whole blood inside blood vessels. However, little literature is devoted to validating the estimation. The goal of this research is to compare the performance of three commonly used methods: the Kubelka-Munk algorithm, optical density algorithm, and inverse Monte Carlo method, for the task of estimating SO<sub>2</sub> from diffuse reflectance spectra. Validation was performed using two data types: Monte Carlo simulated data and *ex vivo* sheep blood that was deoxygenated using sodium dithionite (Na<sub>2</sub>S<sub>2</sub>O<sub>4</sub>). The SO<sub>2</sub> of sheep blood was confirmed using a blood gas analyzer. We measured the diffuse reflectance using two types of HSI cameras: a push-broom and a snapshot HSI camera system. Our results showed that visible wavelengths (400 – 600 nm) are preferred for micro-vessels with diameters less than 100 microns, and near-infrared wavelengths (600 – 900 nm) are preferred for larger vessels. We determined experimentally that sodium dithionite consistently deoxygenated whole blood by 35% for every 1 mg/mL of sodium dithionite to hemoglobin. It was found that the inverse Monte Carlo method performed well in estimating SO<sub>2</sub>, with an average estimation error of 5.53% and 6.97% for *ex vivo* sheep blood and Monte Carlo spectra, respectively. Our findings provide a basis for determining future methods for *in vivo* SO<sub>2</sub> estimations, including surgical HSI applications that rely on accurate perfusion assessment.

**Keywords:** Hyperspectral imaging (HSI), oxygen saturation, surgery, snapshot, near-infrared, sodium dithionite

## 1. INTRODUCTION

The oxygen saturation rate of blood, also known as the oxygenation rate or SO<sub>2</sub> for short, is one of the most important measurements in human physiology [1]. Low SO<sub>2</sub> in the arteries, or hypoxemia, can lead to severe organ damage and is a medical emergency. As such, constant monitoring of SO<sub>2</sub> during medical procedures is important. Formally, oxygenation is calculated as the fraction of hemoglobin binding sites occupied by oxygen [2]. In practice, SO<sub>2</sub> is estimated through optical means [3]. Oxygenated blood appears bright red, whereas deoxygenated blood appears dark, almost brown in color. A low-cost, easy to use device to estimate SO<sub>2</sub> optically is the pulse oximeter [4]. Pulse oximeters are non-invasive, fast, and accurate devices when used on healthy individuals. However, their readings can be skewed in a variety of situations, including high concentrations of methemoglobin, carbon monoxide poisoning, and bronchitis [5].

Hyperspectral imaging (HSI) is a non-invasive imaging modality that can measure spectral values for an entire image. It produces a three-dimensional hypercube, where each layer is a slice of the image taken at a different wavelength. Within the last 20 years, engineering advances have produced hyperspectral cameras that are more compact, perform better, and are cheaper compared to their predecessors [6]. As such, they have found increasingly more uses in various fields, including biological and health sciences. HSI has been used to screen for Alzheimer's disease [7], detect tumors for surgical purposes [8], and predict instances of macular degeneration [9]. SO<sub>2</sub> mapping using HSI is attractive because the method is non-invasive and has advantages over single-point methods such as pulse oximetry. Mordant *et al.* [10] used vessel mapping to show that patients with glaucoma have higher venular SO<sub>2</sub> compared to that of healthy controls. Akbari *et al.* [11] used the mapping technique to detect arteries and veins during surgery. Aref *et al.* [12] used SO<sub>2</sub> vessel mapping to aid phlebotomy.

Many researchers validated their findings in one of two ways. The first is by applying the estimation *in vivo* with healthy subjects to see if the estimated values lie within healthy range [13]. The second is by applying the estimation with 0% and

100% oxygenated blood [14]. However, there is a lack of published work validating intermediate oxygen saturation values using reflectance spectra and HSI. To detect serious physiological conditions such as hypoxia, intermediate oxygenation values must be accurately measured. In this research, we devised schemes to generate blood with intermediate  $SO_2$  values and used HSI to estimate those values. This work also provided a direct comparison and validation of three widely used  $SO_2$  estimation methods across intermediate oxygenation levels to address the gap in current literature.

## 2. METHODS

### 2.1 Acquisition system

We measured the diffuse reflectance spectra of whole blood using a snapshot hyperspectral camera and a spectrometer [15]. The snapshot camera captures images in the red to near-infrared wavelengths (610 – 850 nm). It uses Fabry-Perot interferometers in a  $4 \times 4$  mosaic grid laid on a CMOS sensor. The resulting hypercube is 510 pixels  $\times$  270 pixels  $\times$  16 bands. The spectrometer (Ocean Optics, Florida, USA) measures spectra from 400 – 1000 nm at 1 nm intervals. The spectrometer was placed 5 mm away from the surface of the blood samples. The snapshot camera was connected to a 10 mm,  $0^\circ$  laparoscope (Olympus, Tokyo, Japan), with its tip placed 10 mm away from the surface of the blood samples. The light source used was halogen light. Prior to imaging blood samples, we took a white reference image using a 95% reflective surface (LabSphere, New Hampshire, USA). Figure 1(a) shows the optical setup of the system.

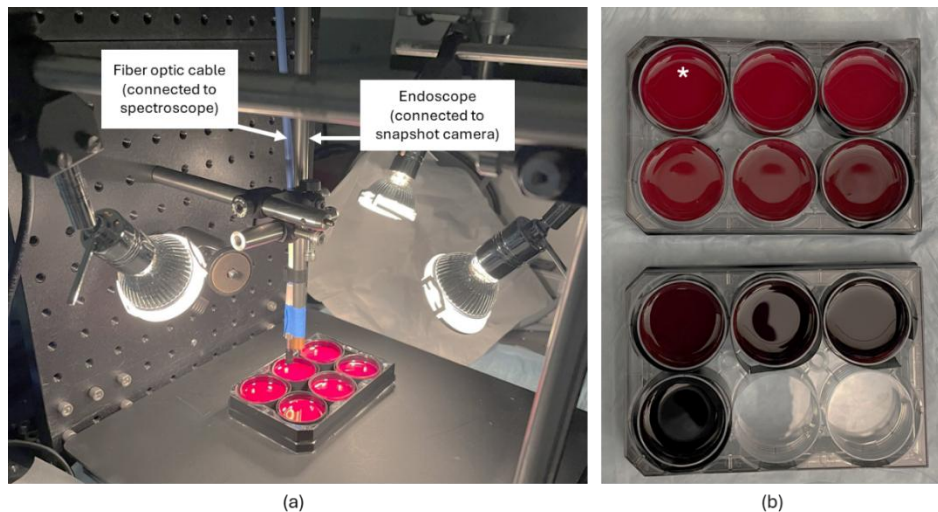


Figure 1. Overview of imaging set up and prepared blood samples for acquisition. (a) Optical setup of the system to acquire hyperspectral images. (b) Blood samples at different concentrations of sodium dithionite. Fully oxygenated blood is marked with a star symbol.

### 2.2 Preparation of blood samples

Defibrinated sheep blood with 36–40% hematocrit (Quad Five, Montana, USA) was used to produce the blood samples for all experiments. Before deoxygenation procedures, the blood was warmed in a  $36^\circ\text{C}$  water bath and exposed to atmospheric air to ensure complete oxygenation. Full oxygenation was confirmed using a Stat Profile Prime Plus Blood Gas Analyzer (BGA, Nova Biomedical, USA). For each BGA measurement, a 0.5 mL blood sample was transferred into a disposable pipette and inserted into the analyzer cartridge for analysis. Two deoxygenation methods were employed: sparging with nitrogen gas and introducing sodium dithionite.

For the nitrogen gas sparging method, a clear vinyl nitrogen hose was inserted directly into the blood. Sparging was performed continuously and periodically paused to collect samples for BGA analysis. Sampling was conducted at intervals of 5, 15, 25, 40, 55, and 70 minutes to monitor the decrease in oxygen saturation. After 70 minutes, the nitrogen flow was

stopped, and the container cap was left open. Over the following 10 minutes, no measurable increase in oxygen saturation was observed.

In the second approach, sodium dithionite ( $\text{Na}_2\text{S}_2\text{O}_4$ ) was used as a chemical deoxygenating agent. Sodium dithionite solution was prepared by dissolving 3.01 g of sodium dithionite salt (Reagents, North Carolina, USA) into 40 mL of 1× phosphate-buffered saline (PBS; Fisher Scientific, Massachusetts, USA) at room temperature and pH 7.4. PBS was selected for its isotonic salinity relative to human blood. To remove dissolved oxygen, the PBS solution was sparged with nitrogen gas for 15 minutes prior to use. A total of 150 mL of fully oxygenated blood was placed in an airtight bottle. A well plate for imaging was prepared by pipetting 1 mL, 3 mL, and 5.5 mL of blood to create samples with respective path lengths of 1 mm, 3 mm, and 5 mm. At the same time, a 0.5 mL sample was collected for BGA analysis. Then, 1 mL of the sodium dithionite–PBS solution, containing 75.25 mg of sodium dithionite, was introduced into the remaining blood volume and stirred thoroughly for 1 minute. The process of extracting samples for imaging preparation, conducting BGA analysis, and stirring with sodium dithionite was repeated until full deoxygenation was observed. Samples with sodium dithionite concentrations of approximately 0, 2.06, 4.10, and 7.15 mg/mL relative to hemoglobin volume were produced after the deoxygenation iterations.

Blood samples at different concentrations appeared progressively darker, as shown in Figure 1(b). To eliminate the spectral contribution of sodium dithionite, the spectral absorbance and reflectance of sodium dithionite solution in PBS were measured at concentrations of 1.0 and 2.0 mg/mL. At these diluted amounts, the sodium dithionite solution did not introduce discernible spectral changes [16].

### 2.3 Hyperspectral image processing

The hyperspectral image was first normalized using a white reference image and a dark reference image. We used the following equation to spectrally correct the image:

$$I = (I_{\text{raw}} - I_{\text{dark}}) / (I_{\text{white}} \times 0.95 - I_{\text{dark}}) \quad (2)$$

where  $I_{\text{raw}}$  is the raw unprocessed spectral image,  $I_{\text{dark}}$  is the dark reference, and  $I_{\text{white}}$  is the image of a white reference tile with a reflectance of 95%. Five images were taken for each blood sample and then averaged to reduce noise. We selected a rectangular region of interest (ROI) for each image of the blood sample and then calculated the average over the ROI to produce the reflectance spectra of blood.

We experimented with standard normal variance (SNV). SNV normalizes the data by ensuring the spectra have a mean of 0 and a standard deviation of 1:

$$I_{\text{after}} = \frac{I - \mu}{\sigma}$$

Here,  $I$  and  $I_{\text{after}}$  are the spectra before and after the normalization;  $\mu$  is the mean spectra, and  $\sigma$  is the standard deviation of the spectra [17].

### 2.4 Estimating $\text{SO}_2$ from diffuse reflectance spectra

We conducted a literature review for a list of commonly used methods to estimate  $\text{SO}_2$  in whole blood. We conducted our investigations on three common methods: Kubelka-Munk, optical density, and inverse Monte Carlo method.

If we assume an infinitely thick layer of blood, the estimated reflectance using Kubelka-Munk became [18, 19]:

$$R(\lambda) = \frac{s(\lambda)}{s(\lambda) + k(\lambda) + 1.5\sqrt{k(\lambda)(k(\lambda) + 2s(\lambda))}} \quad (3)$$

Here,  $s(\lambda)$  is the wavelength-dependent scattering of blood,  $k(\lambda)$  is the wavelength-dependent absorbance, and  $R(\lambda)$  is the wavelength-dependent reflectance. Even though  $s$  is a wavelength-dependent quantity, we set  $s$  to be a constant term for ease of fitting [20]. The absorption coefficients of oxygenated and deoxygenated whole blood came from a literature review by Prahl *et al.* [21] as shown in Figure 2(a).

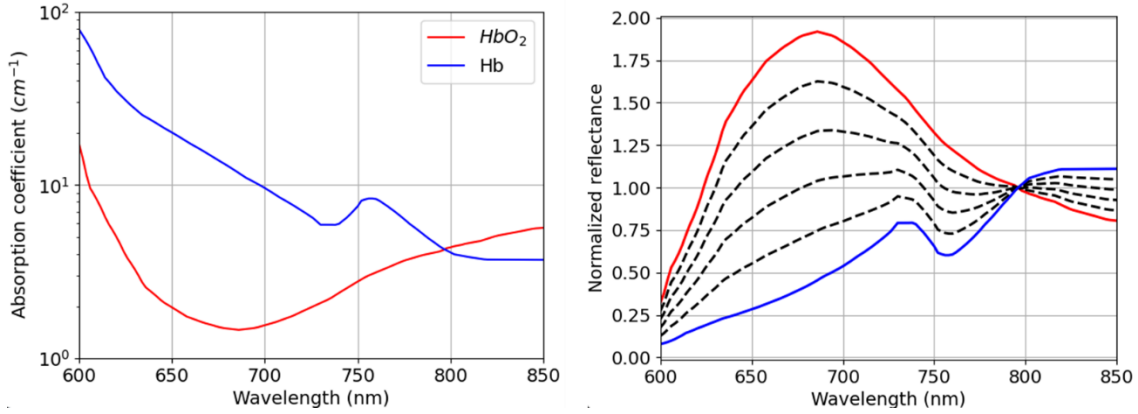


Figure 2. (a) Theoretical absorbance value for oxygenated and deoxygenated hemoglobin from Prahl *et al.* [21] (b) Theoretical reflectance value using Kubelka-Munk theory, using a scattering constant of  $s = 2.2$ . Reflectance values of 80%, 60%, 40%, and 20% oxygenated blood are also plotted as black dashed lines.

The optical density method was commonly seen in literature that used micro-vasculature [22-25]. Here, if the corrected reflectance is  $I$ , then the optical density is:

$$OD = -\log_{10} I$$

Usually, oxygenated and deoxygenated hemoglobin are the two most dominant chromophores in blood. Therefore, many researchers simplified the estimation of  $OD$  as follows:

$$OD = L[HbO_2]\epsilon_{HbO_2} + L[Hb]\epsilon_{Hb} + \alpha$$

Here,  $L$  is the path length,  $\epsilon$  is the molar absorption coefficient of the chromophores,  $\alpha$  is the scattering term,  $[HbO_2]$  is the concentration of oxygenated hemoglobin (arbitrary unit) and  $[Hb]$  is the concentration of deoxygenated hemoglobin. The scattering term is often only a single constant [22-25].

We used least square fitting to find the parameters that minimize the least square error between the estimated and measured spectra. After finding the parameters, the  $SO_2$  value is calculated as follows:

$$SO_2 = \frac{[HbO_2]}{[HbO_2] + [Hb]} \%$$

Here,  $[HbO_2]$  is the concentration of oxygenated hemoglobin (arbitrary unit) and  $[Hb]$  is the concentration of deoxygenated hemoglobin.

## 2.5 Monte Carlo Simulation

Monte Carlo simulations were performed in PyXOpto software [27] to model the diffuse reflectance of whole blood layers over a diffuse reflector. The simulation parameters were chosen to replicate experimental conditions used for whole sheep blood measurements. The model geometry consisted of a top and bottom air layer, and two main layers: a whole-blood layer with variable thicknesses of 1 mm, 3 mm, and 5 mm, and a 25.6 mm Spectralon layer that acted as a diffuse reflecting substrate.

The optical properties of each layer were defined by literature-based parameters (Table 1). Whole blood absorption coefficients ( $\mu_a$ ) were sourced per wavelength using empirical models from Prahl *et al.* [21], assuming an anisotropy factor  $g = 0.95$  and  $n = 1.4$ . Scattering coefficient ( $\mu_s$ ) were estimated using the following theoretical formula:

$$\mu_s(\lambda) = \mu_{500} \left[ f \left( \frac{\lambda}{500} \right)^{-4} + (1-f) \left( \frac{\lambda}{500} \right)^{-b} \right]$$

In this equation,  $\mu_{500}$  is the scattering coefficient of the material at 500 nm,  $\lambda$  is the waveband reported in nm,  $b$  is the Mie scattering power coefficient,  $f$  is the proportion of scattering that belongs to Rayleigh scattering. We used  $\mu_{500} =$

$22 \text{ cm}^{-1}$ , and varied the values of  $f, \lambda, b$ . Spectralon optical properties were set to  $\mu_a = 0.07 \text{ m}^{-1}$  and  $\mu_s = 32\,000 \text{ m}^{-1}$  with  $n = 1.4$  as reported by Majaron et al. [28] Air layers were defined above and below the medium, with refractive index  $n = 1$ .

**Table 1.** Optical properties and geometry for a multi-layer Monte Carlo simulation model of diffuse reflectance for whole blood and Spectralon.

Layer	Optical Parameter				
	Thickness (mm)	Absorption coefficient, $\mu_a$ ( $\text{m}^{-1}$ )	Scattering coefficient, $\mu_s$ ( $\text{m}^{-1}$ )	Anisotropy factor, $g$	$n$
Air (Top)	0	0	0	-	1.0
Whole Blood	1, 3, 5	Wavelength dependent [21]	Wavelength dependent [21]	0.95	1.4
Spectralon	25.6	0.07	32000	0.8	1.4
Air (Bottom)	0	0	0	-	1.0

A collimated line source was positioned at  $(x, y, z) = (0, 0, 0)$  and directed along  $(0, 0, 1)$ , providing normal incidence at the sample surface. The simulation covered the RNIR range (600–900 nm) at 1 nm increments. Each wavelength was simulated independently to account for wavelength-dependent absorption and scattering. A total of  $1 \times 10^6$  photon packets were launched for each run to ensure statistical convergence with less than 1% Monte Carlo noise. Photon packets were terminated when traveling beyond 10 cm from the source.

Monte Carlo simulation was used to generate simulations with varying  $\text{SO}_2, f, \lambda,$  and  $b$  values. A total of 9,801 simulations were generated. The simulations were gathered into a lookup table. To find the oxygenation value of our reflectance data, we found the simulated reflectance that minimized the RMSE difference between it and the measured data.

Diffuse reflectance was recorded using a radial integrating-sphere detector with an opening radius of 0.5 cm. The detector accumulated photon packets within a 1 cm diameter region, divided into two radial bins (0–1 cm), allowing total reflected photon collection through the top surface. Simulations were run on a 64-bit system equipped with 32-core AMD Epyc 7502 CPUs and an NVIDIA RTX A6000 GPU (48 GB memory). PyXOpto version 1.2 was used with OpenCL acceleration for parallel photon propagation.

### 3. RESULTS

#### 3.1 Oxygenation rate correlated with concentration of sodium dithionite

We reported very little difference in the diffuse reflectance between sheep blood deoxygenated using nitrogen gas and sodium dithionite. The similarities were confirmed through both reflectance and absorption spectra of samples with closely matched  $\text{SO}_2$  values.

Deoxygenation using nitrogen gas sparging progressed slowly, measuring 27%  $\text{SO}_2$  after approximately 70 minutes. In contrast, the deoxygenation process using sodium dithionite was much faster, only involving one minute of stirring during each reagent addition interval. This demonstrates that sodium dithionite achieves full deoxygenation in a fraction of the time required for nitrogen sparging.

By measuring the changes in the sodium concentration using the blood gas analyzer, we found that our experiment produced an average yield of 90%. For every 1 mg/mL of  $\text{Na}_2\text{S}_2\text{O}_4$  added relative to hemoglobin volume,  $\text{SO}_2$  decreased by approximately 16%. Briely-Sabo et al. [29] found that for every 1 mg/g of  $\text{Na}_2\text{S}_2\text{O}_4$  added to whole blood, blood is deoxygenated by 35%. Assuming a hematocrit of 45% by volume [30] and a whole-blood density of 1.06 g/mL, their result corresponds to roughly 14.9% deoxygenation per 1 mg/mL relative to hemoglobin volume, which closely matches our findings. In Figure 3, the correlation between  $\text{SO}_2$  and concentration of sodium dithionite in blood was plotted. The graph shows a strong linear relationship with an  $R^2$  value of 0.9823.

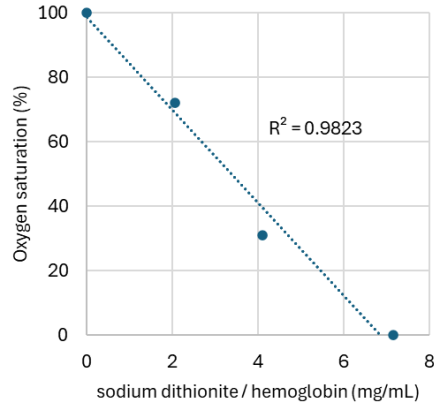


Figure 3. Correlation between SO<sub>2</sub> and concentration of sodium dithionite in blood.

Spectral comparisons were performed using data collected from nitrogen gas deoxygenation and the sodium dithionite deoxygenation procedures. Spectra with similar SO<sub>2</sub> values were paired at depths of 1 mm, 3 mm, and 5 mm (100% vs. 99%, 72% vs. 74%, and 27% vs. 31%, respectively). Figure 4 shows a comparison of spectra acquired with both methods at 1 mm depth. After normalizing each spectrum to its maximum reflectance, the two methods showed very similar spectral shapes across all depths.

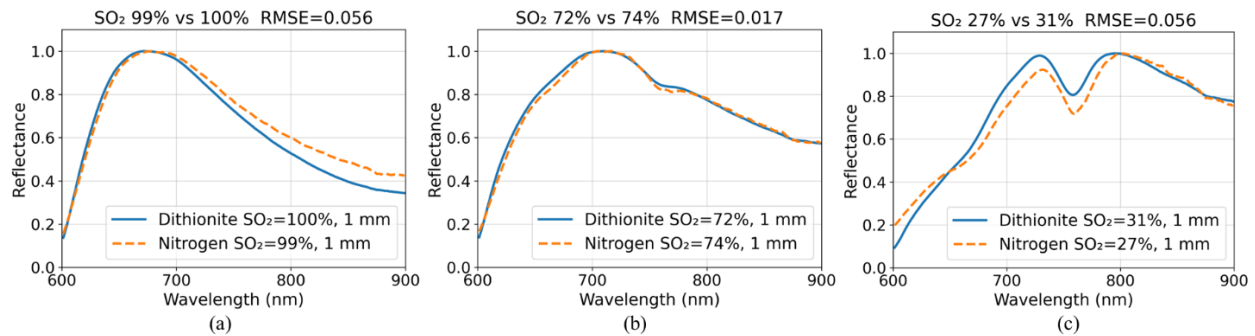


Figure 4. Comparison of spectra acquired by nitrogen gas sparging and sodium dithionite deoxygenation procedure at similar levels of oxygen saturation. The spectra of diffuse reflectance for both methods were normalized by their maximum values, then RMSE was calculated between each pair in (a), (b), and (c).

To quantify similarity, the root mean square error (RMSE) was calculated using the formula:

$$RMSE = \sqrt{\frac{\sum_{i=1}^n (D_i - N_i)^2}{n}}$$

where  $D_i$  and  $N_i$  denote the normalized reflectance values at wavelength index  $i$  for the sodium dithionite method sample and the nitrogen-sparged sample, respectively, and  $n$  is the total number of sampled wavelengths across the measured spectral range. RMSE values between the normalized spectra ranged from 0.017 to 0.079 across the measured depths of 1 mm, 3 mm, and 5 mm, indicating strong overall agreement between values obtained from sodium dithionite and nitrogen gas-based deoxygenation.

### 3.2 Path length affects the diffuse reflectance

In Figure 5, the experimental diffuse reflectance spectra are shown for four different oxygenation rates: 100%, 72%, 31%, and 0% for path lengths of 1, 3, and 5 mm. Fully oxygenated whole blood has a reflectance peak located at around 650

nm, whereas fully deoxygenated blood has two reflectance peaks at 730 and 800 nm. These spectral changes are characteristic of the transition from oxyhemoglobin to deoxyhemoglobin. Increasing the optical path length reduces overall reflectance intensity; the 1 mm curves show slightly stronger feature contrast, while the 3 mm and 5 mm spectra are similar in amplitude.

The corresponding Monte Carlo RNIR simulations were generated using the same oxygenation conditions and path lengths in Figure 6. The simulated results closely reproduce the experimental spectral reflectance patterns. The influence of optical path length in the simulations also aligns with the experimental observations, with decreasing intensity as depth increases and overall spectral shape being preserved.

Figures 7 and 8 show the experimental and simulated visible range spectra, respectively. In Figure 7, the experimental visible range spectra exhibit distinct peaks and troughs between 500 and 600 nm at 100% SO<sub>2</sub>, followed by a rise toward a plateau after 600 nm. As the blood deoxygenates, these features smooth into a broad peak near 480 nm, with intensity decreasing until 550 nm, then climbing through 650 nm. Increasing the path length (0.01–0.05 mm) reduces intensity and gradually suppresses fine spectral features. Figure 8 shows that these visible range reflectance trends are again closely replicated in the Monte Carlo results.

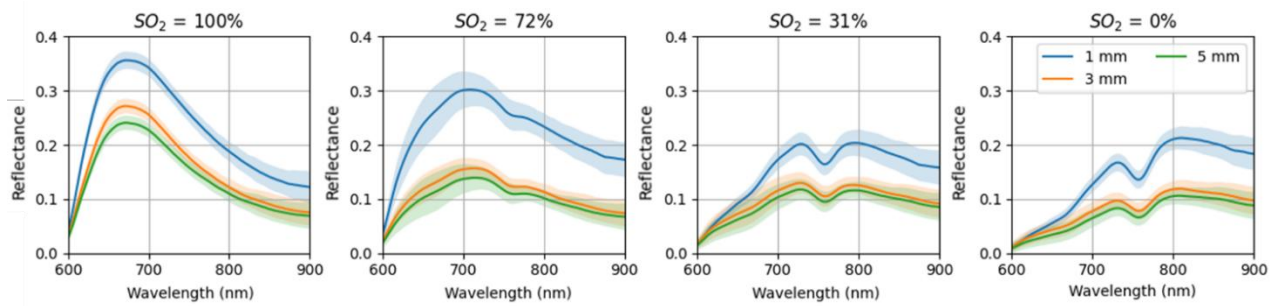


Figure 5. Experimental RNIR reflectance spectra of whole sheep blood at SO<sub>2</sub> levels of 100%, 72%, 31%, and 0% for path lengths of 1, 3, and 5 mm.

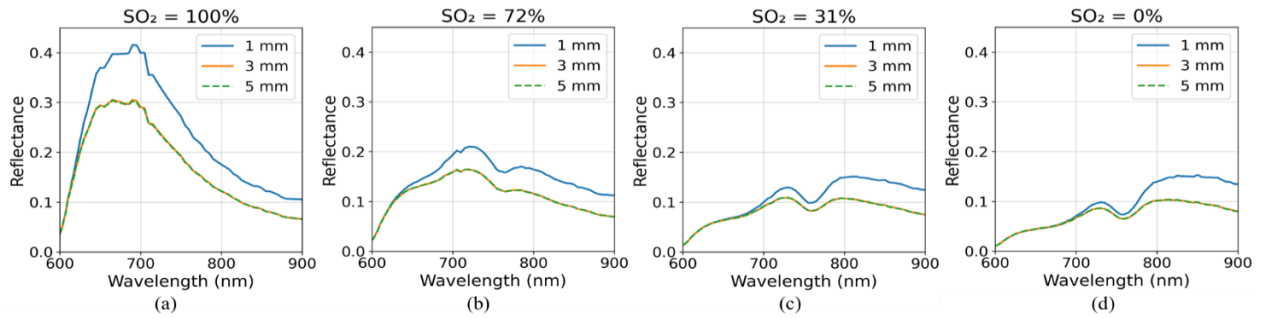


Figure 6. Monte Carlo-simulated RNIR reflectance spectra at SO<sub>2</sub> levels of 100%, 72%, 31%, and 0% for path lengths of 1, 3, and 5 mm.

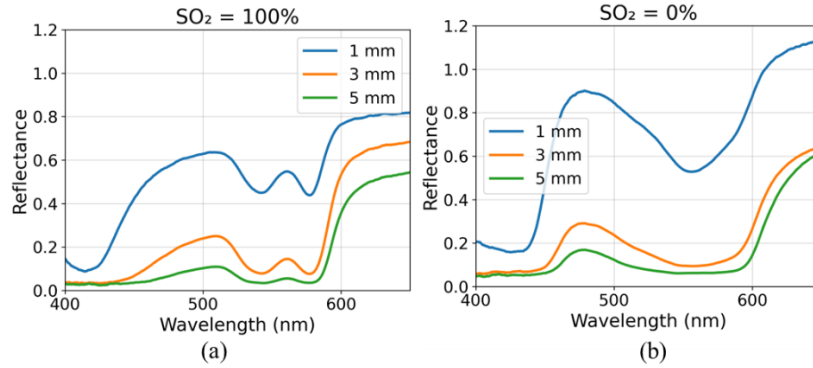


Figure 7. Experimental visible reflectance spectra of whole sheep blood at SO<sub>2</sub> levels of 100% and 0% for path lengths of 1, 3, and 5 mm.

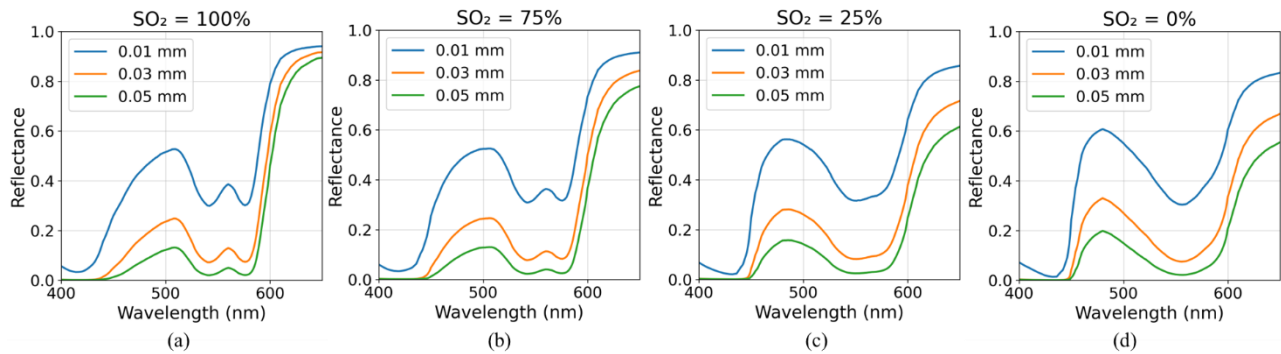


Figure 8. Monte Carlo-simulated visible reflectance spectra at SO<sub>2</sub> levels of 100%, 75%, 25%, and 0% for path lengths of 0.01, 0.03, and 0.05 mm.

### 3.3 Estimation results

Table 2 and Table 3 show the estimation error for three different methods, on both *ex vivo* sheep blood and Monte Carlo simulated samples. We note that inverse Monte Carlo method produces SO<sub>2</sub> estimates with the lowest errors, yielding an average error of  $9.9 \pm 9.7\%$ ,  $3.6 \pm 2.2\%$ ,  $3.1 \pm 2.9\%$  on *ex vivo* sheep blood at depths of 1 mm, 3 mm, and 5 mm, respectively, and  $11.5 \pm 8.4\%$ ,  $4.6 \pm 2.6\%$ ,  $4.8 \pm 2.4\%$  for Monte Carlo simulated data. Diving deeper into the performances, we found that all methods were able to correctly estimate the SO<sub>2</sub> when the oxygenation rate was at 100% or 0%. In Figure 9, the fitted reflectance curves at 99% SO<sub>2</sub> closely matched the measured spectra for all methods, which display a pronounced peak near 690 nm. However, as oxygenation decreased to intermediate levels (approximately 61% SO<sub>2</sub>), the spectral peak shifted toward 710 nm and a distinct dip emerged around 750 nm. Under these conditions, the Kubelka-Munk and inverse Monte Carlo methods more accurately captured the spectral shape changes associated with hemoglobin deoxygenation, whereas the optical density method consistently underestimated SO<sub>2</sub> values when the SO<sub>2</sub> was between 20 – 80% (Figure 10).

Table 2. Average error for different estimation methods on whole sheep blood samples. The unit of error is in absolute oxygen saturation percentage points.

Depths	Estimation method		
	Kubelka-Munk	Optical density	Inverse Monte Carlo
1 mm	$15.2 \pm 13.2 \%$	$11.1 \pm 9.2 \%$	$9.9 \pm 9.7 \%$
3 mm	$18.7 \pm 13.5 \%$	$13.0 \pm 13.7 \%$	$3.6 \pm 2.2 \%$
5 mm	$13.9 \pm 11.2 \%$	$18.7 \pm 17.9 \%$	$3.1 \pm 2.9 \%$

Table 3. Average error for different estimation methods on Monte Carlo simulated samples. The unit of error is in absolute oxygen saturation percentage points.

Depths	Estimation method		
	Kubelka-Munk	Optical density	Inverse Monte Carlo
1 mm	$6.6 \pm 2.7 \%$	$14.9 \pm 12.7 \%$	$11.5 \pm 8.4 \%$
3 mm	$22.0 \pm 11.9 \%$	$22.0 \pm 14.7 \%$	$4.6 \pm 2.6 \%$
5 mm	$22.1 \pm 12.0 \%$	$22.1 \pm 14.8 \%$	$4.8 \pm 2.4 \%$

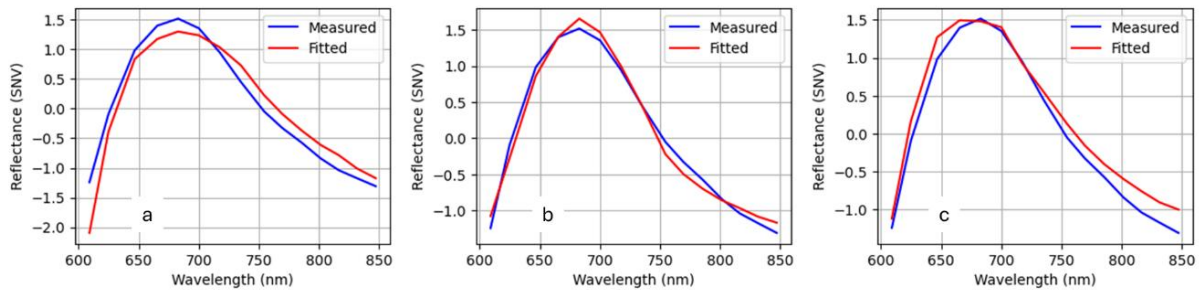


Figure 9. Fit curves of (a) optical density method, (b) Kubelka-Munk method and (c) Inverse Monte Carlo method where the ground truth  $\text{SO}_2$  is 99%.

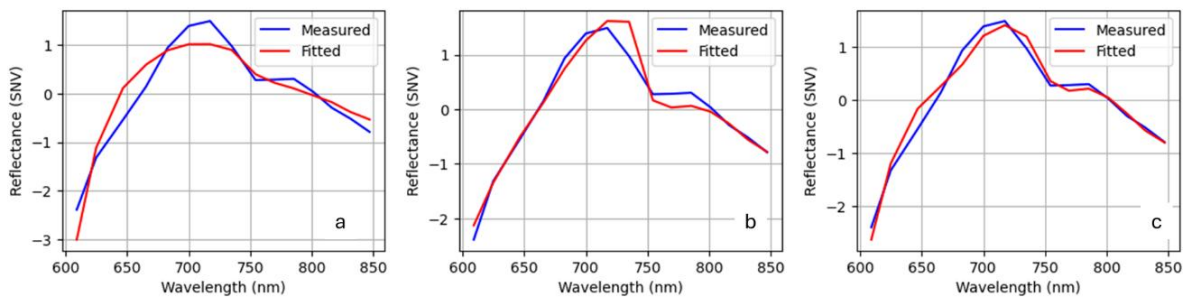


Figure 10. Fit curves of (a) optical density method, (b) Kubelka-Munk method and (c) Inverse Monte Carlo method where the ground truth  $\text{SO}_2$  is 61%.

#### 4. DISCUSSION AND CONCLUSION

In this study, we present a robust method for generating controlled  $\text{SO}_2$  values and using these values to validate three commonly used  $\text{SO}_2$ -estimation algorithms for diffuse reflectance hyperspectral imaging. This goal was achieved through the development of a sodium-dithionite protocol capable of producing stable  $\text{SO}_2$  levels from 0 to 100 percent, confirmed using a blood gas analyzer. Accurate  $\text{SO}_2$  validation is essential for hyperspectral imaging research because reflectance-based  $\text{SO}_2$  maps rely directly on the relationship between measured spectra and true oxygenation. Without intermediate validation points, algorithm performance cannot be meaningfully compared or optimized.

Despite the widespread use of sodium dithionite for blood deoxygenation [31, 32], current dithionite protocols vary widely in mixing steps, concentration ratios, and timing. Such variability introduces reproducibility issues for  $\text{SO}_2$  values across studies and limits the ability to compare findings in the literature. Our protocol addresses this gap by producing predictable  $\text{SO}_2$  reductions per unit dithionite concentration, yielding consistent linear behavior across all trials. The ability to generate

controlled SO<sub>2</sub> levels enables systematic evaluation of hyperspectral cameras and SO<sub>2</sub>-estimation algorithms under matched spectral conditions. We focused on the clinical relevance of our method, as oxygenation rates in patients typically range from 40% to 100%. Validating this interval is especially important for applications such as tissue perfusion assessment, vessel identification, and intraoperative decision-making. Among the three algorithms tested, the inverse Monte Carlo method performed best at intermediate oxygenation values. This method assumes a thin-slab optical model, which better matches the behavior of whole blood in vessel-scale geometries compared to infinitely thick approximations such as Kubelka–Munk. The improved fit was evident in both experimental and Monte Carlo datasets, especially between 40% and 80% SO<sub>2</sub>. We believe that this method holds promise in future estimations of whole blood within vessels.

The positioning and angle of the endoscope tip may also influence the spectra. Small changes in imaging geometry alter photon path length and the relative contributions of forward scattering and backscattering, which can shift spectral intensity. The inclusion of a Spectralon layer in the Monte Carlo simulations enabled the simulated reflectance to capture the combined absorption and scattering behavior of the full imaging system rather than the blood layer alone. The effect was most pronounced at shallow blood depths, where a significant fraction of detected photons interacted with the underlying background. Additionally, thicker blood layers (~5 mm) produced stronger multiple-scattering effects than vessel-scale layers (~1 mm), consistent with the reduced feature contrast observed in Figures 5–7. By separating geometric, scattering, and thickness-dependent contributions, the Monte Carlo simulations provide a framework for refining spectral corrections for whole-blood samples and scaling results toward small-vessel measurements.

In clinical settings, having a validated SO<sub>2</sub> protocol is valuable for developing and testing new hyperspectral systems intended for surgical guidance or diagnostic use. Controlled SO<sub>2</sub> samples allow researchers to evaluate algorithm accuracy before moving to in vivo or intraoperative studies, strengthening the reliability of device performance and supporting eventual clinical translation.

This study acknowledges several limitations. Our experiments used sheep blood with a fixed hematocrit range, which may not fully represent the optical properties of human blood across all clinical presentations. Instrument-specific factors, such as illumination geometry and sensor noise, may also influence reflectance. Although Monte Carlo simulations successfully reproduced spectral trends, they rely on literature-based optical properties and may not capture all sources of experimental variability when translated to real clinical values. Future work may focus on refining the sodium-dithionite protocol to further improve mixing uniformity and batch-to-batch consistency of the experiment. Comparisons of Monte Carlo diffuse reflectance results can be performed against in vivo reflectance values at different SO<sub>2</sub> measurements in animal or human tissues. Monte Carlo modeling can also be expanded to isolate additional factors such as vessel thickness, imaging geometry, and scattering contributions. By incorporating simulation-derived corrections, future computational models may compensate for practical variations in imaging conditions and enhance the accuracy of SO<sub>2</sub> estimation in hyperspectral imaging.

## ACKNOWLEDGEMENTS

Research reported in this publication was supported in part by the National Cancer Institute of the National Institutes of Health under Award Number R01CA288379 and R01CA204254, the Cancer Prevention and Research Institute of Texas (CPRIT) under Award Number RP240289 and RP240542, and the Eugene McDermott Graduate Fellowship (EMGF) 202009 at the University of Texas at Dallas. The content is solely the responsibility of the authors and does not necessarily represent the official views of the National Institutes of Health.

## REFERENCES

- [1] B. Hafen, and S. Sharma, [Oxygen Saturation] Treasure Island, FL, 11/23/2022 (2024).
- [2] K. D. McClatchey, [Clinical Laboratory Medicine] Lippincott Williams & Wilkins, 370 (2002).
- [3] N. Bosschaart *et al.*, “A literature review and novel theoretical approach on the optical properties of whole blood,” *Lasers in Medical Science*, 29(2), 453-479 (2014).
- [4] M. Nitzan *et al.*, “Pulse oximetry: fundamentals and technology update,” *Medical Devices: Evidence and Research*, 7(null), 231-239 (2014).
- [5] J. E. Sinex, “Pulse oximetry: Principles and limitations,” *The American Journal of Emergency Medicine*, 17(1), 59-66 (1999).

- [6] M. H. Tran, and B. Fei, "Compact and ultracompact spectral imagers: technology and applications in biomedical imaging," *Journal of Biomedical Optics*, 28(4), 040901 (2023).
- [7] X. Hadoux *et al.*, "Non-invasive in vivo hyperspectral imaging of the retina for potential biomarker use in Alzheimer's disease," *Nature Communications*, 10(1), 4227 (2019).
- [8] B. Fei *et al.*, "Label-free reflectance hyperspectral imaging for tumor margin assessment: a pilot study on surgical specimens of cancer patients," *Journal of Biomedical Optics*, 22(8), 086009 (2017).
- [9] N. Lee *et al.*, "In vivo snapshot hyperspectral image analysis of age-related macular degeneration." *Int Conf IEEE Eng Med Biol Soc*, 5363-5366 (2010).
- [10] D. J. Mordant *et al.*, "Oxygen saturation measurements of the retinal vasculature in treated asymmetrical primary open-angle glaucoma using hyperspectral imaging," *Eye*, 28(10), 1190-1200 (2014).
- [11] H. Akbari *et al.*, "Blood vessel detection and artery-vein differentiation using hyperspectral imaging." 1461-1464.
- [12] M. H. Fouad Aref *et al.*, "Delineation of the Arm Blood Vessels Utilizing Hyperspectral Imaging to Assist with Phlebotomy for Exploiting the Cutaneous Tissue Oxygen Concentration," *Photodiagnosis and Photodynamic Therapy*, 33, 102190 (2021).
- [13] S. Singh *et al.*, "Development and Validation of Non simultaneous Retinal Image Acquisition–Based Retinal Oximeter," *Scientific Reports*, 7(1), 4270 (2017).
- [14] J. Kaluzny *et al.*, "Bayer Filter Snapshot Hyperspectral Fundus Camera for Human Retinal Imaging," *Current Eye Research*, 42(4), 629-635 (2017).
- [15] K. Pruitt *et al.*, "A high-speed hyperspectral laparoscopic imaging system." *Proc SPIE Int Soc Opt Eng*, 12466, 1246608 (2023).
- [16] K. Dalziel, and J. R. O'Brien, "Side reactions in the deoxygenation of dilute oxyhaemoglobin solutions by sodium dithionite," *Biochem J*, 67(1), 119-24 (1957).
- [17] S. N. Mohapatra, and C. W. Smith, "Infrared isobestic region for whole blood," *Medical and biological engineering*, 13(6), 929-931 (1975).
- [18] A. Hoefft *et al.*, "In Vivo Measurement Of Blood Oxygen Saturation By Analysis Of Whole Blood Reflectance Spectra." *Proc SPIE Int Soc Opt Eng*, 1067, 62-68 (1989).
- [19] L. Gevaux *et al.*, "Three-dimensional maps of human skin properties on full face with shadows using 3-D hyperspectral imaging," *Journal of Biomedical Optics*, 24(6), 066002 (2019).
- [20] N. T. Clancy *et al.*, "Intraoperative colon perfusion assessment using multispectral imaging," *Biomedical Optics Express*, 12(12), 7556-7567 (2021).
- [21] S. Prahl, [Optical absorption of hemoglobin], [http://omlc.ogi.edu/spectra/hemoglobin\(1999\)](http://omlc.ogi.edu/spectra/hemoglobin(1999)).
- [22] K. J. Zuzak *et al.*, "Visible Reflectance Hyperspectral Imaging: Characterization of a Noninvasive, in Vivo System for Determining Tissue Perfusion," *Analytical Chemistry*, 74(9), 2021-2028 (2002).
- [23] B. Sorg *et al.*, "Hyperspectral imaging of hemoglobin saturation in tumor microvasculature and tumor hypoxia development," *Journal of Biomedical Optics*, 10(4), 044004 (2005).
- [24] S. P. Nighswander-Rempel *et al.*, "Mapping tissue oxygenation in the beating heart with near-infrared spectroscopic imaging," *Vibrational Spectroscopy*, 32(1), 85-94 (2003).
- [25] N. T. Clancy *et al.*, "Intraoperative measurement of bowel oxygen saturation using a multispectral imaging laparoscope," *Biomedical Optics Express*, 6(10), 4179-4190 (2015).
- [26] S. Prahl, "Everything I think you should know about Inverse Adding-Doubling," *Oregon Medical Laser Center, St. Vincent Hospital*, 1344, 1-74 (2011).
- [27] P. Naglič *et al.*, "pyxopto: An Open-Source Python Library with Utilities for Fast Light Propagation Modeling in Turbid Media," *OSA Technical Digest, paper EM3C.2* (2021).
- [28] Majaron, B. and Žel, T., *Optical properties of Spectralon assessed by replication of literature data in Monte Carlo simulations* (SPIE Photonics Europe). SPIE, 2022.
- [29] K. Briely-Sabo, and A. Bjornerud, "Accurate de-oxygenation of ex vivo whole blood using sodium Dithionite." *Proc Intl Soc Mag Reson Med*, 8, (2000).
- [30] H. H. Billett, [Hemoglobin and hematocrit] Butterworths, Boston, 151 (1990).
- [31] A. S. Luthman *et al.*, "Bimodal reflectance and fluorescence multispectral endoscopy based on spectrally resolving detector arrays," *Journal of Biomedical Optics*, 24(3), 031009 (2018).
- [32] G. Lu *et al.*, "Estimation of tissue optical parameters with hyperspectral imaging and spectral unmixing," *Proc SPIE Int Soc Opt Eng*, 9417, 94170Q (2015).